Inertial Effects on Rotating Flow in a Porous Layer

D. N. Riahi
Department of Theoretical and Applied Mechanics
216 Talbot Laboratory, 104 South Wright Street
University of Illinois at Urbana-Champaign
Urbana, Illinois 61801 U. S. A.
(Email: d-riahi@uiuc.edu)

Abstract

Inertial effects on flow instabilities in a horizontal reactive porous layer with deformed upper boundary are studied using a linear stability analysis and under the condition that the porous layer, which is also referred to as a dendrite or mushy layer, is rotating about an inclined axis during the solidification of a binary alloy. The linear stability analysis leads to new results about the effects of the inertial force on the existence and the number of the oscillatory modes and on the preference of either left- or right-traveling longitudinal rolls, which can depend on the angle of inclination γ of the rotation axis with respect to the vertical axis. For some $0°<\gamma<90°$ and for the rotation rate beyond some particular value, the preferred flow solution in the form of left-traveling rolls can be replaced by the one in the form of right-traveling rolls or vice-versa. The preferred flow pattern, the period of oscillation of the flow solution, the critical Rayleigh number and the shape and structure of the deformed upper boundary of the layer are found to depend on the inertial effect.

NOMENCLATURE

a	horizontal wave number	$\boldsymbol{a}$	horizontal wave number vector
a_c	critical a	a_1	x component of $\boldsymbol{a}$
a_2	y component of $\boldsymbol{a}$	C	scaled concentration ratio
c	center of gravity	$\tilde{C}$	dimensional composition
C_0	far-field composition	C_e	eutectic composition
C_l	specific heat	C_r	a concentration ratio
C_s	composition of the dendrites	g	acceleration due to gravity
G	$1+S/C$	G_t	$(G\text{-}1)/(CG^2)$
h	non-dimensional thickness of the porous layer	$\tilde{h}$	porous layer thickness
		i	pure imaginary number
k	thermal diffusivity	k_s	solute diffusivity
K	a permeability ratio	K_1	a permeability parameter
K_2	a permeability parameter	$\tilde{L}$	an inertial parameter
L	scaled inertial parameter	L_a	latent heat of solidification

N_g	acceleration due to high gravity	P	scaled modified pressure
$\tilde{P}$	modified pressure	$\boldsymbol{r}$	position vector
R	scaled Rayleigh number	$\tilde{R}$	Rayleigh number
R_c	critical R	$\tilde{S}$	non-dimensional concentration
S	scaled Stefan number	S_t	Stefan number
t	scaled time variable	T	Coriolis parameter
$\tilde{t}$	time variable	$\tilde{T}$	temperature
T_e	eutectic temperature	T_L	liquidus temperature
T_∞	far-field temperature	$\boldsymbol{u}$	scaled volume flux per unit area
$\boldsymbol{U}$	velocity vector	$\tilde{\boldsymbol{u}}$	volume flux per unit area
$\tilde{u}$	x component of $\tilde{\boldsymbol{u}}$	W	poloidal function for $\boldsymbol{u}$
V_0	solidification speed	$\tilde{v}$	y component of $\tilde{\boldsymbol{u}}$
$\tilde{w}$	z component of $\tilde{\boldsymbol{u}}$	x	scaled horizontal variable
$\boldsymbol{x}$	unit vector along x-axis	$\tilde{x}$	horizontal variable
y	scaled horizontal variable	$\boldsymbol{y}$	unit vector along y-axis
$\tilde{y}$	horizontal variable	z	scaled vertical variable
$\boldsymbol{z}$	unit vector along z-axis	$\tilde{z}$	vertical variable

Greek symbols

α^*	thermal expansion coefficient	β^*	solute expansion coefficient
β	$\beta^*-\Gamma\alpha^*$	Γ	liquidus slope
ΔC	$C_0 - C_e$	ΔT	$T_L(C_0)-T_e$
Δ_2	horizontal Laplacian operator	δ	value of h in the absence of motion
η	$h-\delta$	η'	constant coefficient
ε	inverse of a Lewis number	∇	gradient operator
$\tilde{\theta}$	non-dimensional temperature	θ	perturbation temperature
θ_B	basic temperature	θ_i	interface temperature
θ_∞	$[T_\infty - T_L(C_0)]/\Delta T$	θ'	z-dependent coefficient for θ
ν	kinematic viscosity	Ω	rotation rate
$\boldsymbol{\Omega}$	rotation vector	γ	inclination angle
Π	permeability	ϕ	perturbation to solid fraction
ϕ_B	basic solid fraction	$\tilde{\phi}$	local solid fraction
ϕ'	z-dependent coefficient for ϕ	ψ	toroidal function for $\boldsymbol{u}$
ψ'	z-dependent coefficient for ψ	σ	complex growth rate
σ_i	disturbance frequency	σ_r	real growth rate

1. Introduction

About one decade ago Anderson and Worster (1996) carried out linear stability analysis for convective flow in a horizontal mushy layer during alloy solidification in the absence of rotating and inertial effects. They identified an oscillatory instability under certain conditions on the range of values of some parameters of the problem. Their investigation was based on a single-layer model of the mushy zone due to Amberg and Homsy (1993). Such model was under a near-eutectic approximation in the limit of large far-field temperature, and it was assumed that the mushy layer is bounded by two

horizontal rigid and flat boundaries. Thus, such a single-layer model did not include any effects of a liquid layer, which usually lies over the mushy layer in a binary-alloy solidification system (Worster 1992). However, as pointed out by Amberg and Homsy (1993) and Anderson and Worster (1995, 1996) and is also evident from the results due to Chung and Chen (2000), such a mushy-layer model can provide the main qualitative results about the mushy-layer mode of convection, which are expected to hold in an actual two-layer system (Worster 1992).

The oscillatory instability detected by Anderson and Worster (1996) was distinct from that found by Chen et al. (1994), which arose due to double-diffusive convection in a two-layer system in which stabilizing thermal buoyancy was present. The mushy-layer model treated by Anderson and Worster (1996) did not have double-diffusive effects, due to strong coupling between the solute and thermal fields, which was imposed by the condition of thermodynamic equilibrium. The Anderson-Worster oscillatory instability was due to a mechanism internal to the mushy layer and in the absence of any double-diffusive effect, and it implied existence of an important interaction between convection, solidification and heat transfer.

Recently Riahi (2005), hereafter referred to as R5, investigated the flow instabilities in a horizontal dendrite layer with deformed stress-free upper boundary and rotating about an inclined axis during alloy solidification and in the absence of inertial effects. His linear stability analysis provided results, in particular, about the critical mode of convection, neutral stability curve, preferred flow pattern and the shape of the deformed upper boundary. The results also uncovered a new oscillatory instability, which was due to the horizontal component of the rotation axis. About the oscillatory instabilities detected in R5, it should be noted that the author took into account the assumptions that were used by Anderson and Worster (1996) and by Amberg and Homsy (1993) in their non-rotating system to study the rotating problem. It was found that the oscillatory instability, due to Anderson and Worster (1996), was enhanced by the presence of rotation, and, in addition, it was detected a new oscillatory instability, which could even operate in the parameter regime studied by Amberg and Homsy (1993) where no oscillatory instability was possible.

In the problem studied in R5, some effects of the overlying liquid layer was taken into account by assuming that a motionless liquid layer lies over the mushy layer, so that the mush-liquid interface is treated realistically as a deformed free surface. The author then employed some realistic boundary conditions between the dendrite and liquid layer to determine both the flow solution in the dendrite layer and the shape of the surface on top of the dendrite layer. The information about the morphology of the mush-liquid interface can be significant in the model treated in R5 since infinite degeneracy of the linear solutions is removed completely by the presence of the horizontal component of the rotation vector leading to preferred flow solution and preferred structure of the mush-liquid interface, which can be of interest in the geophysical applications, such as implications with respect to the observed earth's inner-core anisotropy (Bergman 1997), which is one of the major unsolved problem about the earth's deep interior.

In the present study we revisited the problem treated in R5 but with the inertial effects included and found some interesting new results. In particular, we found that inertial effects can eliminate Anderson-Worster type oscillatory instability but unable to eliminate the oscillatory instability due to the horizontal component of rotation, even though such instability can be modified by the inertial force. In addition, for some values of the angle of inclination γ of the rotation axis with respect to the vertical axis, the preferred flow pattern and the shape of the moving deformed upper boundary can change from right-traveling rolls to left-traveling rolls or vice versa for the value of the rotation rate just above some value.

The numerical evaluation of the analytical expressions for the Anderson-Worster oscillatory mode derived in R5 was based on the approximate value of 3.14 for π, which also was a singular point in the equation for the frequency. It turns out that such approximate value for π favors the singular point as non-removable, while sufficiently exact value for π, such as 3.141592654, leads to a removable singular point for π. In the present paper we also have taken into account this point, which can make a difference for the value of the frequency close to π, and updated two figures 4 and 6 in R5 accordingly.

2. Governing system

We consider a horizontal layer of a binary alloy melt of some constant composition C_0 and temperature T_∞, which is cooled from below and is solidified at a constant speed V_0, with the eutectic temperature T_e at the position $\tilde{z}=0$ held fixed in a frame moving with the solidification speed in the vertical $\tilde{z}$-direction (Figure 1). As in R5, the solidifying system is assumed to be rotating at a constant speed Ω about a unit vector $\mathbf{\Omega}$, which is inclined at an angle γ with respect to the vertical $\tilde{z}$-axis. Here $\tilde{z}$-axis is anti-parallel to the gravity vector. Within the layer of melt, there is a dendrite layer adjacent to the solidifying surface and of thickness $\tilde{h}(\tilde{x}, \tilde{y}, \tilde{t})$, where the solid dendrites and the liquid melt coexist. Here $\tilde{t}$ is time variable, and $\tilde{x}$ and $\tilde{y}$ are the horizontal variables along the $\tilde{x}$- and $\tilde{y}$-axes in the horizontal plane $\tilde{z}=0$.

As discussed in R5, particular applications of the present problem can be in geophysics and engineering. In engineering, material processing in high gravity is a relevant example (Regel and Wilcox, 1997; Riahi, 1997). Here the solidifying system is placed in a centrifuge rotating at some angular velocity Ω about the centrifuge axis, which makes the angle γ with respect to the vertical axis. The centrifuge axis is anti-parallel to the earth's gravity vector, and the vertical axis is anti-parallel to the high-gravity vector, which is the result of the superposition of the earth's gravity vector and the centrifugal force of the center of mass c of the solidification system. Figure 2 presents such a solidification system in a centrifuge. Here the effective gravity vector for the solidification system is that due to the high-gravity vector, which is anti-parallel to the scaled vertical axis (z-axis).

In this paper we focus on the so-called mushy-layer mode (Worster 1992) at the onset of convection for the flow within the dendrite layer only. It should also be noted

that such layer is considered to be in local thermodynamic equilibrium and, thus, a linear relation between the temperature $\tilde{T}$ and the composition $\tilde{C}$ in the dendrite layer is assumed (Worster 1992).

Next, we consider the equations for momentum, continuity, heat and solute for both liquid region ($\tilde{z}>\tilde{h}$), which is assumed to be motionless, and dendrite region ($0<\tilde{z}<\tilde{h}$) in the frame $o\tilde{x}\tilde{y}\tilde{z}$ moving with the solid-mush interface ($\tilde{z}=0$) at speed V_0 and rotating with the solidifying system at the constant angular velocity Ω. In contrast to the problem studied in R5, we retain the inertial terms in the momentum equation, which can be appropriate in the cases of liquid metals where the Prandtl number is sufficiently small as explained in Vadasz (1998). The governing system is non-dimensionalized by using V_0, k/V_0, k/V_0^2, $\beta\Delta C\rho_0 gk/V_0$, ΔC and ΔT as scales for velocity, length, time, pressure, solute and temperature, respectively. Here k is the thermal diffusivity, ρ_0 is a reference (constant) density, $\beta=\beta^*-\Gamma\alpha^*$, α^* and β^* are the expansion coefficients for the heat and solute respectively and the slope of the liquidus Γ is assumed to be constant, $\Delta C=C_0-C_e$, $\Delta T=T_L(C_0)-T_e$, T_L is the liquidus temperature and C_e is the eutectic composition. Just as in the experimental studies of Sample and Hellawell (1984), where the effect of the centrifugal force was found to be negligible, we shall assume that the ratio of centrifugal force to the gravity-driven buoyancy force is sufficiently small, so that the rotational effects are important only through the presence of the Coriolis force and the angle of inclination γ.

The non-dimensional form of the equations for momentum, temperature and solute concentration in the liquid layer in the motionless state, where the continuity equation is satisfied identically, are

$$\nabla\tilde{P}+R\tilde{S}\boldsymbol{z}=0, \tag{1a}$$

$$(\partial/\partial\tilde{t}-\partial/\partial\tilde{z})\tilde{\theta}=\nabla^2\tilde{\theta}, \tag{1b}$$

$$(\partial/\partial\tilde{t}-\partial/\partial\tilde{z})\tilde{S}=\varepsilon\nabla^2\tilde{S}, \tag{1c}$$

where $\tilde{P}$ is the modified pressure, R is the Rayleigh number to be defined in the next paragraph, $\tilde{S}$ is the non-dimensional concentration, $\tilde{\theta}$ is the non-dimensional temperature, $\varepsilon=k_s/k$ is the inverse of a Lewis number, k_s is the solute diffusivity, $\boldsymbol{z}$ is a unit vector in the positive direction of the $\tilde{z}$-axis, and for simplicity of notation, all the non-dimensional independent variables are designated by their dimensional symbols. The parameter ε is assumed to be small as is the case in the applications.

The non-dimensional form of the equations for momentum, continuity, temperature and solute concentration in the porous layer, which is assumed to be under Darcy's law (Roberts and Loper 1983; Fowler 1985; Worster 1991), are

$$\{[\tilde{L}/(1-\tilde{\phi})](\partial/\partial\tilde{t}-\partial/\partial\tilde{z})+K(\tilde{\phi})\}\tilde{\boldsymbol{u}}=-\nabla\tilde{P}-\tilde{R}\,\tilde{\theta}\,\boldsymbol{z}+T\,\tilde{\boldsymbol{u}}\times\boldsymbol{\Omega}/(1-\tilde{\phi}), \tag{2a}$$

$$\nabla.\tilde{\mathbf{u}} = 0, \tag{2b}$$

$$(\partial/\partial\tilde{t} - \partial/\partial\tilde{z})(\tilde{\theta} - S_t\tilde{\phi}) + \tilde{\boldsymbol{u}}.\nabla\tilde{\theta} = \nabla^2\tilde{\theta}, \tag{2c}$$

$$(\partial/\partial\tilde{t} - \partial/\partial\tilde{z})[(1-\tilde{\phi})\tilde{\theta} + C_r\tilde{\phi}] + \tilde{\boldsymbol{u}}.\nabla\tilde{\theta} = 0, \tag{2d}$$

where $\boldsymbol{\Omega}=cos(\gamma)\mathbf{z}+sin(\gamma)\mathbf{x}$ is the rotation vector, $\tilde{\boldsymbol{u}}=\tilde{u}\boldsymbol{x}+\tilde{v}\boldsymbol{y}+\tilde{w}\boldsymbol{z} = (1-\tilde{\phi})\boldsymbol{U}$ is the volume flux per unit area (Worster, 1992), $\tilde{\phi}$ is the local solid fraction within the dendrite layer, $\boldsymbol{U}$ is the velocity vector, $\tilde{u}$ and $\tilde{v}$ are the horizontal components of $\tilde{\boldsymbol{u}}$ along the $\tilde{x}$- and $\tilde{y}$-directions, respectively, $\boldsymbol{x}$ and $\boldsymbol{y}$ are unit vectors along the positive $\tilde{x}$- and $\tilde{y}$-directions, $\tilde{w}$ is the vertical component of $\tilde{\boldsymbol{u}}$ along the $\tilde{z}$-direction, $\tilde{\theta}$ is the non-dimensional temperature or non-dimensional composition (R5), $\tilde{R}=\beta\Delta C g\Pi(0)/(V_0\nu)$ is the Rayleigh number, $\Pi(0)$ is reference value at $\tilde{\phi}=0$ of the permeability $\Pi(\tilde{\phi})$ of the porous medium, ν is the kinematic viscosity, g is acceleration due to gravity, $\tilde{L}=V_0^2\Pi(0)/(k\nu)$ is an inertial parameter, $K(\tilde{\phi})\equiv\Pi(0)/\Pi(\tilde{\phi})$, $S_t=L_a/(C_l\,\Delta T)$ is the Stefan number, C_l is the specific heat per unit volume, L_a is the latent heat of solidification per unit volume, $C_r=(C_s-C_0)/\Delta C$ is a concentration ratio, C_s is the composition of the solid phase forming the dendrites and $T=2\Omega\Pi(0)/\nu$ is the Coriolis parameter (square root of a Taylor number). The equation (2d) is based on the limit of sufficiently large value of the Lewis number.

The governing equations (1)-(2) are subject to the following boundary conditions:

$$\tilde{\theta}+1=\tilde{w} = 0 \quad \text{at} \quad \tilde{z} = 0, \tag{3a}$$

$$[\tilde{\theta}]=[\boldsymbol{n}.\nabla\tilde{\theta}]=[\boldsymbol{n}.\tilde{\boldsymbol{u}}]=\tilde{\phi}=0 \quad \text{at} \quad \tilde{z} = h, \tag{3b}$$

$$\tilde{\theta}\to\theta_\infty,\ \tilde{S}\to 0 \text{ as } z\to\infty, \tag{3c}$$

where the square brackets denote the jump in the enclosed quantity across the mush-liquid interface, $\boldsymbol{n}$ is a unit vector normal to the interface, $h=\tilde{h}V_0/k$ is the dimensionless depth of the dendrite layer and θ_∞ is the non-dimensional form of T_∞.

Following Amberg and Homsy (1993) and Anderson and Worster (1996) in reducing the model asymptotically, we assume certain rescaling to be given below in the limit of sufficiently small δ, where δ is the assumed constant value of h in the absence of motion.

$$C_r=C/\delta,\ S_t=S/\delta,\ \tilde{L}=L/\delta^2,\ \delta<<1, \tag{4a}$$

$$(\tilde{x},\tilde{y},\tilde{z})=\delta(x,y,z),\quad \tilde{t}=\delta^2 t,\quad R^2=\delta\tilde{R}\ , \tag{4b}$$

$$\tilde{\boldsymbol{u}}=R\boldsymbol{u}/\delta,\quad \tilde{P}=RP, \tag{4c}$$

where C and S are order one quantities, and L is either an order one or an order less than one quantity as $\delta\to 0$· As discussed in Anderson and Worster (1996), the assumption of

thin dendrite layer ($\delta<<1$) is associated with the large non-dimensional far-field temperature, which can occur when the initial $\tilde{C}$ is close to C_e. The assumption of order one quantity C corresponds to the near-eutectic approximation (Fowler 1985), which allows one to describe the dendrite layer as a porous layer of constant permeability to the leading order. The assumption of order one quantity S allowed Anderson and Worster (1996) to detect a new oscillatory instability from their analytical mushy-layer model, while only stationary instability is possible if S is of order less than unity (Anderson and Worster 1995). The assumption considered for L is consistent with the realistic range of values of the temporal derivative of the volume flux as discussed in Vadasz (1998) for the liquid metal cases.

The rescaling (4a)-(4c) are then used in the governing system (1)-(3). The resulting system of equations and boundary conditions admits a motionless basic state, which is steady and horizontally uniform. The basic state solution, denoted by the subscript 'B', is the same as the one given in R5 and will not be repeated here. The basic state solution involves a composite parameter $G \equiv S/C+1$ and is assumed to be valid in the limits of

$$\varepsilon<<\delta,\ \varepsilon^2<<1/R. \tag{5}$$

Since $\tilde{\phi}$ is expected to be small, according to the results (6e), the following expansion for $K(\tilde{\phi})$ will be implemented later in the governing system:

$$K(\tilde{\phi})=1+K_1\tilde{\phi}+K_2\tilde{\phi}^{\,2}+\ldots., \tag{6}$$

where the coefficients K_1 and K_2 are constants.

Just like the zero-inertial case treated in R5, we use the general representation

$$\boldsymbol{u}=\nabla\times(\nabla\times\boldsymbol{z}W)+\nabla\times\boldsymbol{z}\psi \tag{7}$$

for the divergence-free vector field $\boldsymbol{u}$ (Chandrasekhar 1961). Here W and ψ are the poloidal and toroidal functions for $\boldsymbol{u}$, respectively. Taking the vertical components of the curl and the double –curl of the Darcy's momentum equation (2a) and using the expressions for the basic state variables and (5)-(7) in (2)-(3), we find the following leading order system for the dependent variables of the infinitesimal disturbances superimposed on the basic state for the flow in the porous layer:

$$[1+\delta(1-z)/C]L(\partial/\partial t-\delta\partial/\partial z)\nabla^2\Delta_2 W-(\delta/C)L(\partial/\partial t-\delta\partial/\partial z)\Delta_2 W+\Delta_2\nabla^2\{[1+K_1\delta(1-z)/C]W\}+(\delta$$

$$K_1/C)\Delta_2\partial W/\partial z-\Delta_2\theta+T\Delta_2[sin(\gamma)\partial/\partial x+cos(\gamma)\partial/\partial z]\{\psi[1+\delta(1-z)/C]\}-(T\,\delta/C)sin(\gamma)$$

$$\Delta_2\partial W/\partial y=0, \tag{8a}$$

$$[1+\delta(1-z)/C]L(\partial/\partial t-\delta\partial/\partial z)\Delta_2\psi+\Delta_2\{[1+K_1\delta(1-z)/C]\psi\}-T[1+\delta(1-z)/C]\{\Delta_2[sin(\gamma)\,\partial/\partial x+$$

$$cos(\gamma)\partial/\partial z]W\}=0, \tag{8b}$$

$$(\partial/\partial t-\delta\partial/\partial z)[-\theta+(S/\delta)\phi]+R[1+\delta G(1-2z)/2]\Delta_2 W+\nabla^2\theta=0, \tag{8c}$$

$$(-\partial/\partial t+\delta\partial/\partial z)\{[1-\delta(1-z)/C]\theta+[(1-z)+\delta G(z^2-z)/2]\phi+(C/\delta)\phi\}+[1+$$

$$\delta G(1-2z)/2]\Delta_2 W=0, \tag{8d}$$

$$\theta=W=0 \quad \text{at} \quad z=0, \tag{8e}$$

$$\partial\theta/\partial z-\eta=\theta=W=\phi=0 \quad \text{at} \quad z=1, \tag{8f}$$

where

$$\eta=h-\delta,\ \Delta_2=\partial^2/\partial x^2+\partial^2/\partial y^2 \tag{8g}$$

and

$$(\theta,\ \phi)=(\tilde{\theta}-\theta_B,\ \tilde{\phi}-\phi_B). \tag{8h}$$

3. Analysis

The analysis carried out for the present problem is similar to that presented in R5 and, thus, briefly described here. We first seek normal mode type solution of the form

$$(W,\ \psi,\ \theta,\ \phi,\ \eta)=[W'(z),\ \psi'(z),\ \theta'(z),\ \phi'(z),\ \eta']\exp(\sigma t+i\,\boldsymbol{a}.\boldsymbol{r}), \tag{9}$$

where $\sigma=\sigma_r+i\sigma_i$ is the complex growth rate, i is the pure imaginary number ($\sqrt{-1}$), σ_r is the real growth rate, σ_i is the frequency of the disturbances, $\boldsymbol{r}=(x, y)$ is the horizontal position vector, $\boldsymbol{a}=(a_1, a_2)$ is the horizontal wave number vector of the disturbances and $a=|\boldsymbol{a}|$ is the horizontal wave number. Here a_1 and a_2 are the x- and y-components of $\boldsymbol{a}$, respectively. Using (9) in (8), we find a system of ordinary differential equations and boundary conditions for the z-dependent coefficients W', ψ', θ' and ϕ', and, in addition, the result

$$d\theta'/dz=\eta' \quad \text{at} \quad z=1 \tag{10}$$

for the constant coefficient η' given in (9) is followed. The function $\eta(x, y, t)$, which provides the shape of the structure of the top free surface of the porous layer, will be determined once the disturbance system is solved analytically.

Next, we consider the following expansions of the dependent variables and parameters in powers of δ:

$$(W', \psi', \theta', \phi', R, \sigma_r, \sigma_i)=(W_0, \psi_0, \theta_0, \phi_0, R_0, \sigma_{r0}, \sigma_{i0})+$$

$$\delta(W_1, \psi_1, \theta_1, \phi_1, R_1, \sigma_{r1}, \sigma_{i1})+\ldots \tag{11}$$

Using (11) in the system for the z-dependent coefficients, we solve the resulting systems in the orders $1/\delta$, δ^0 and δ^1 to determine the main stability results. The systems to the orders $1/\delta$ and δ and their subsequent analysis, including that for the minimization process at the marginally stable state, are the same as those given in R5 and will not be repeated here. The results are

$$\sigma_{r0}= \sigma_{i0}=0. \tag{12a}$$

$$a_1=0. \tag{12b}$$

$$W_0 =[(\pi^2+a_2^2)/(R_0 a_2^2 G)]sin(\pi z), \tag{12a}$$

$$\psi_0=T\pi\, cos\gamma\, [(\pi^2+a_2^2)/(R_0 a_2^2 G)]cos(\pi z), \tag{12b}$$

$$\theta_0= - sin(\pi z), \tag{12c}$$

$$\phi_0=\{-\pi(\pi^2+a_2^2)/(CG[(\sigma_{r1}+i\sigma_{i1})^2+\pi^2])\}\{[(\sigma_{r1}+i\sigma_{i1})/\pi]sin(\pi z)+cos(\pi z)+exp[(\sigma_{r1}+i\sigma_{i1})(z-1)]\}, \tag{12d}$$

$$R_0^2=(\pi^2+a_2^2)[(\pi^2+a_2^2)+(\pi Tcos\gamma)^2]/(a_2^2 G). \tag{12e}$$

$$R_{0c}= \pi\{1+[1+(Tcos\gamma)^2]^{1/2}\}/\sqrt{G}, \tag{12f}$$

$$a_c= \pi[1+(Tcos\gamma)^2]^{1/4}, \tag{12g}$$

where R_{0c} is the minimum value of R_0 achieved at $a_2 =a_c$. The result (12b) implies preference of the shape of the upper boundary and the flow pattern within the porous layer in the form of two-dimensional traveling rolls whose axes are parallel to the *x*-axis.

At order δ we find the simplified system for W_1 and θ_1 after eliminating ψ_1 and ϕ_1 between all the four equations. We then multiply the equation for W_1 by $Ga_2^2 W_0$ and equation for θ_1 by θ_0, add the resulting equations, integrate over the fluid layer and make use of the boundary conditions. The result is a complex equation whose real and imaginary parts for the neutrally stable flow case, where $\sigma_{r1} =0$, yield

$(R_1/R_0)=[K_1/(4C)]\{[\pi^2+a_2^2-(\pi T\cos\gamma)^2]/[\pi^2+a_2^2+(\pi T\cos\gamma)^2]+(\pi T\cos\gamma)^2/[2C(\pi^2+a_2^2)+2C($

$\pi T\cos\gamma)^2]+GG_t\{1/4+ \pi^2[1+\cos(\sigma_{i1})]/(\pi^2-\sigma_{i1}^2)^2\}$, (13a)

$\sigma_{i1}\{1+G_t[(\pi^2+a_2^2)/(\pi^2-\sigma_{i1}^2)][1-2\pi^2\sin\sigma_{i1}/(\sigma_{i1}\pi^2-\sigma_{i1}^3)]+L(\pi^2+a_2^2)^2[\pi^2+a_2^2-\pi^2T^2\cos^2(\gamma)]/($

$R_0Ga_2)^2\}+T\sin\gamma(\pi^2+a_2^2)^2/(a_2CG^2R_0^2)=0$, (13b)

where $G_t=(G-1)/(CG^2)$.

4. Results and discussion

It can be seen from (13b) that zero value of the frequency is not possible in the presence of inclined rotation where T and γ are non-zero, and, thus, the case with inclined rotation admits only oscillatory type solutions. To investigate the kind of oscillatory instabilities that can occur in the present problem, we numerically evaluated the solutions with non-zero frequency of (13b). Figures 3 and 4 present, respectively, the cases of L=0 and 0.05 for the frequency of the neutrally stable oscillatory modes versus T in the range $0\le T\le 10$ for G=2 and G_t= 0.672. The solid, dashed and dotted lines in each figure correspond, respectively, to the cases of γ=0°, 30° and 60°. Although our main focus in this paper is on the results in the presence of the inertial effects where $L\neq 0$, we also would like to consider and discus the case with L=0 (figure 3) because it could show more clearly the effects of the inertial force for the corresponding case with non-zero L (figure 4), and, in addition, the results presented in the figure 3 provide an updating results of the figure 4 in R5. As explained briefly in the section 1, the results of numerical evaluation of the analytical expressions reported in R5, which were based on the approximate value of 3.14 of π, did not adequately provide the results for the actual cases where the value of the frequency was sufficiently close to π. Hence, the results reported in R5 were altogether satisfactory with the exception of those which were for the value of the frequency sufficiently close to π, such as those provided in the figures 4 and 6 of that paper. In both of those two figures in R5, the values of π=3.14 and G_t=0.2 were used which turn out to correspond to the accurate values of π=3.141592654 and G_t =0.672 in the present numerical calculation.

First consider the vertical rotation case where γ=0°. It can be seen from either the figure 3 or the figure 4 in the present paper that there are two oscillatory modes, one a mirror image of another with respect to σ_{i1}=0. Hence, left-traveling solution, (where the phase velocity of the solution is in the direction opposite to that of the component of the position vector along the wave-number vector), right-traveling solution, (where the phase velocity of the solution is in the direction of the component of the position vector along the wave-number vector) and standing solution can all be possible neutrally stable modes for the case of γ=0°. But as can be seen from the figure 4, no oscillatory mode was possible for T=0 or $T\ge 5$. Hence, inertial effect tends to reduce the domain for the presence of the oscillatory mode. In addition, a comparison between the results presented

in these 2 figures indicate that in the range $0.5 \leq T \leq 4.5$ where the oscillatory mode exists in the presence or absence of the inertial force, the period of oscillation of the flow for the case with the inertial force included is higher, but the period of oscillation decreases with increasing the rotation rate regardless of the inertial effect.

Next, let us consider a particular case of inclined rotation where $\gamma=30°$. The corresponding graphs (dashed lines) shown in the figures 3 and 4 indicate the results that are given as follow. For either in the absence or in the presence of the inertial force, there are three distinct oscillatory modes two of which with $\sigma_{i1}>0$ and one with $\sigma_{i1}<0$. Hence, each of the two modes with positive frequency corresponds to the solution in the form of left-traveling rolls, while the mode with negative frequency corresponds to the solution in the form of right-traveling rolls. In the absence of the inertial effect there are at least one or at most three oscillatory modes for a given T in the studied range [0, 10]. There exist particular values of T below which the preferred flow pattern or shape of the upper free boundary surface is in the form of right-traveling rolls and above which such oscillatory rolls are replaced by the left-traveling rolls, or vice-versa. Such results are concluded after the critical value R_c is evaluated at such neighboring points. Also, across such points the period of oscillation of the preferred solution changes abruptly to a different value. The period of oscillation for the mode with a negative frequency and for the mode with the largest positive frequency decrease with increasing T, while that for the mode with the smallest positive frequency increases with T. In the presence of the inertial effect the main results, which are provided by the figure 4, are as follow. For sufficiently small rotation rate ($T<<1$), there is no oscillatory mode. There are at most two oscillatory modes for a given T in the range [0, 10]. There exist particular values of T below which the preferred flow cells or upper boundary shape is in the form of left-traveling rolls and above which such oscillatory rolls are replaced by the right-traveling rolls, or vice versa. There exist also particular values of T below which the preferred flow pattern or shape of the upper free-boundary is in the form of left-traveling rolls and above which the period of oscillation of such rolls increases abruptly. The period of the oscillation for the mode with a negative frequency and for the mode with the larger positive frequency decreases with increasing T, while that for the mode with the smaller positive frequency increases with T.

For a larger value of the angle of inclination, such as $\gamma=60°$, the figures 3 and 4 provide such notable results, which are given as follow. The figure 3 shows that for $\gamma=60°$ there is only one oscillatory mode with negative frequency, which corresponds to the solution in the form of right-traveling rolls. The period of oscillation for this mode decreases with increasing the rotation rate, and the rate of change of the period of oscillation with the rotation rate also decreases with increasing the rotation rate. When the inertial effect is included (figure 4), there is again only one oscillatory mode with negative frequency for the preferred solution in the form of right-traveling rolls. But now the period of oscillation decreases slowly with increasing the rotation rate if the rotation rate is small and decreases rapidly with increasing the rotation rate if the rotation rate is large. The rate of change of the period of oscillation with the ration rate increases with the rotation rate if the inertial effect is included.

The results presented in the figures 3 and 4 are in a sense representative results of our frequency calculation for different values of the parameters. It was also found that the magnitude of the frequency of the critical mode decreases with increasing S or C since S=C. Similar to the case in the absence of the inertial effects (R5), the results indicate presence of two different oscillatory instabilities. The first one is the rotational extension of the one discovered by Anderson and Worster (1996), which is present in both cases of inclined ($\gamma \neq 0$) and vertical (γ=0) rotation, and such instability, referred to here as Anderson-Worster oscillatory instability. It is due to an interaction between convection, solidification and heat transfer within the dendrite layer. Our results in the presence of the inertial effects indicate that such oscillatory instability is enhanced by the presence of rotation. The second type of oscillatory instability was referred to in R5 as a new instability due to the presence of the horizontal component of the rotation vector. The results presented in the figure 4, which are generally for the frequency of the combined of these two oscillatory instability mechanisms, indicate that the magnitude of the frequency as well as the magnitude of the rate of change of the frequency with respect to T, due to Anderson-Worster oscillatory instability, increases with T.

To determine the preference of the critical mode of convection, we needed to examine the expression for the critical value R_c for R given by

$$R_c = R_{0c} + \delta R_{1c} + O(\delta^2), \tag{14}$$

where R_{0c} is given by (12f), and R_{1c} is given by (13a), provided R_0, a and σ_{i1} are replaced , respectively, by R_{0c} , given by (12f), a_c, given by (12g), and σ_{i1} for the most critical mode. Figures 5 and 6 are the same as the figures 3 and 4, respectively, but for R_c instead of the frequency. It can be seen from these 2 figures that rotation is stabilizing, while the inclination angle is destabilizing. The rate of increase of the critical Rayleigh number with respect to the rotation rate decreases with increasing the angle of inclination. In the presence of the inertial effects, no oscillatory mode is possible for large rotation rate if the external rotation is vertical. The result (12g) indicates that the critical value a_c of a also increases with T. Hence, in both cases in the presence or absence of the inertial effects, the rotational constraint exerts stabilizing effect on the most critical mode of convection at the onset of motion. Also, the rotational constraint through the Coriolis force reduces the wavelength of the preferred mode since a_c increases with T. In addition, R_c decreases with increasing S or γ, while a_c decreases with increasing γ and is independent with respect to either S or C.

We also examined the vertical distribution of the perturbation to the solid fraction for a critical mode in the absence and presence of the inertial effects. Some typical results are presented in Figure 7, in the absence of the inertial effect, and in Figure 8, in the presence of the inertial effect, for the vertical distribution of the perturbation to the solid fraction, which can provide information for the tendency for the chimney formation in the dendrite layer if the value of the perturbation ϕ to the solid fraction is negative, while tendency for the enhancement of the dendrite solid in the layer follows if the value of ϕ is positive. For these figures, G=2, G_t=0.672, K_1=1.0, δ =0.2 and the value of 0.01 is chosen for the amplitude of the perturbation quantities. It should be noted that the value

of G_t=0.672 in the present study corresponding to the value of the 3.18 for the frequency in the absence of rotation is calculated from the equation (13b) for the frequency based on the sufficiently accurate value of π=3.141592654, so that the present figure 5 for L=0 is the updated one for the figure 6 in R5. Figure 7 presents the results for ϕ versus z for the preferred mode at $y = t$=L=0, G=2.0 and G_t=0.672. Here the solid, dashed and dotted lines present, respectively, the cases for (T, γ)= (0.0, 0.°), (1.0, 0.°) and (1.0, 60.°). It can be seen from this figure that in the absence of rotation ϕ is negative throughout the layer, except at a very small region adjacent to the lower boundary. In the region where ϕ is negative the magnitude $|\phi|$ increases with z over about lower one-quarter of the layer and decreases with increasing z over the rest of the layer. For the vertical and inclined rotation cases (dashed line and dotted line), ϕ is positive over about lower 15% and 35% of the layer, respectively, and negative elsewhere. These results clearly indicate that the tendency for the chimneys formation can be reduced more in the dendrite layer by the inclined rotational effects. Figure 8 presents the results for ϕ versus z as in the case of figure 7 but for L=0.05. It can be seen from this figure that ϕ is negative throughout the layer for both in the absence and in the vertical rotation cases, while ϕ is positive over about lower 25% of the layer in the case of inclined rotation. This result is in agreement with the experimental observation (Sample and Hellawell 1984) that the chimney formation can be reduced by the application of an inclined rotation at moderate rotation rate. Our calculated data for the preferred oscillatory mode also indicate that the vertical location of the occurrence for the chimney-formation tendency can change with time. Thus, it is quite possible that the directions of the chimneys that could develop in a dendrite layer in a time-dependent flow be non-vertical.

The calculated data based on the results (12f), (13a) and (14) indicated also that for C=S, R_c increases with either L or K_1 and decreases with increasing S for given T. Physically, these results can be explained as follows. Since K_1 is generally positive and is a representation of the inverse of the permeability of the dendrite layer, then the present system is expected to stabilize as K_1 increases. Similar to the Coriolis force, the inertial force tends to counteract the buoyancy force and, thus, has stabilizing effect on the flow system. Since S represents a measure of the latent heat relative to the heat content and C represents the difference in the characteristic composition of the solid and liquid phases to the compositional variation of the liquid, then in the present case of S=C the destabilizing effect of S dominated over the stabilizing effect of C.

4. Conclusion

The results based on a linear stability analysis of flow in a horizontal porous layer rotating about an inclined axis and in the presence of inertial effects that depending on the rotation rate and the angle of inclination of the rotation axis with the vertical axis the preferred flow within the dendrite layer and the shape of the deformed upper boundary can be in the form of left- or right-traveling longitudinal rolls. For some angle of inclination and for the rotation rate beyond some particular value, the preferred flow solution in the form of left-traveling rolls can be replaced by the one in the form of right-traveling rolls or vice-versa. The preferred form of the flow solution, the period of

oscillation of the preferred flow pattern, the critical Rayleigh number at the onset of motion and the shape of the deformed upper boundary can all depend on the inertial effects. The effects of the Coriolis force, due to the inclined rotational constraint at moderate rotation rate, can generally be stabilizing and, hence, beneficial in a number of industrial and engineering applications. Presence of inclined rotation is found to reduce the tendency for the chimney formation in the dendrite layer. This later result is in agreement with the experimental results (Sample and Hellawell 1984). Under the inclined rotational constraint, the realized structure for the surface on top of the dendrite layer is that of longitudinal traveling rolls, which is found to be the same as the preferred flow pattern in the present problem.

REFERENCES

Amberg, G. and Homsy, G. M., Nonlinear analysis of buoyant convection in binary solidification with application to channel formation, *J. Fluid Mech*., Vol. 252, pp. 79-98, 1993.

Anderson, D. M. and Worster, G. M., Weakly nonlinear analysis of convection in mushy layers during the solidification of binary alloys, *J. Fluid Mech*., Vol. 302, pp. 307-331, 1995.

Anderson, D. M. and Worster, G. M., A new oscillatory instability in a mushy layer during the solidification of binary alloys, *J. Fluid Mech*., vol. 307, pp. 245-267, 1996.

Bergman, M. I., Measurements of electric anisotropy due to solidification texturing and the implications for the Earth's inner core, *Nature*, vol. 389, pp. 60-63, 1997.

Chandrasekhar, S., *Hydrodynamic and Hydromagnetic Stability*, Oxford University Press, Oxford, 1961.

Chen, F., Lu, J. W. and Yang, T. L., Convective instability in ammonium chloride solution directionally solidified from below, *J. Fluid Mech*., vol. 276, pp.163-187, 1994.

Chung, C. A. and Chen, F., Onset of plume convection in mushy layers, *J. Fluid Mech*., vol. 408, pp. 53-82, 2000.

Fowler, A. C., The formation of freckles in binary alloys, *IMA J. Appl. Maths*., vol. 35, pp. 159-174, 1985.

Regel, L. L. and Wilcox, W. R., *Centrifugal Materials Processing,* L. L. Regel and W. R. Wilcox (eds.), Plenum Press, New York, pp. 1-15, 1997.

Riahi, D. N., Effects of centrifugal and Coriolis forces on chimney convection during alloy solidification, *J. Crystal Growth*, vol. 179, pp. 287-296, 1997.

Riahi, D. N., Flow instabilities in a horizontal dendrite layer rotating about an inclined axis, *J. Porous Media*, vol. 8, pp. 327-342, 2005.

Roberts, P. H. and Loper, D. E., Towards a theory of the structure and evolution of a dendrite layer, *Stellar and Planetary Magnetism*, A. M. Soward (ed.), Gordon and Breach, New York, pp. 329-349, 1983.

Sample, A. K. and Hellawell, A., The mechanisms of formation and prevention of channel segregation during alloy solidification, *Met. Trans. A.*, vol. 15, pp. 2163-2173, 1984.

Vadasz, P., Coriolis effect on gravity-driven convection in a rotating porous layer heated from below, *J. Fluid Mech.*, vol. 376, pp. 351-375, 1998.

Worster, M. G., Natural convection in a mushy layer, *J. Fluid Mech.*, vol. 224, pp. 335-359, 1991.

Worster, M. G., Instabilities of the liquid and mushy regions during solidification of alloys, *J. Fluid Mech.*, vol. 237, pp. 649-669, 1992.

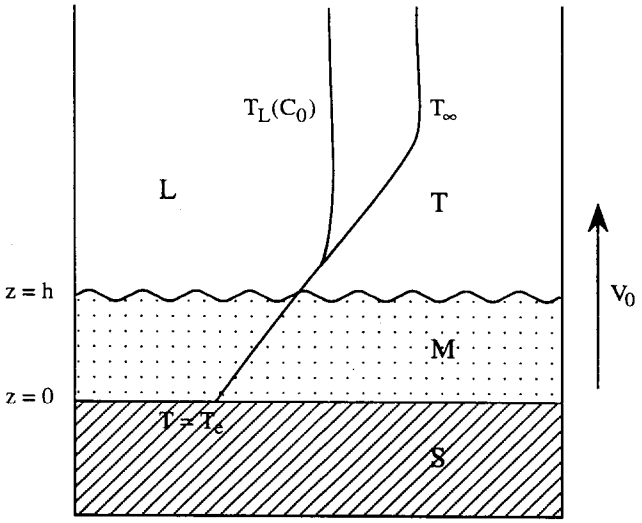

Figure 1. A diagram representing the directional solidification of an alloy at speed V_0. A mushy (dendrite) layer between a solid region, where $T<T_e$, and a liquid region. The profiles for dimensional temperature and the local liquidus temperature T_L are also shown. L, M, and S denote, respectively, liquid, mush, and solid regions.

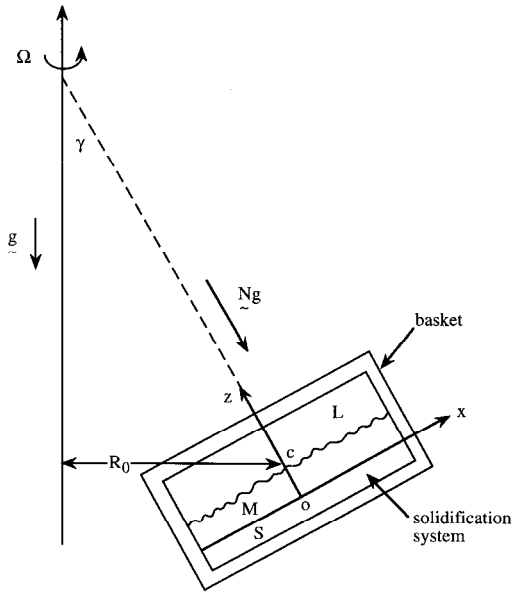

Figure 2. Diagram representing the solidification in a centrifuge together with the coordinate system, effective gravity vector, inclination angle, and rotation vector.

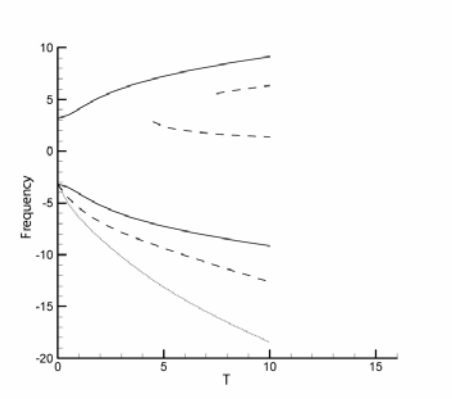

Figure 3. Frequency versus T for L=0, G=2.0 and G_t=0.672. Here the solid, dashed and dotted lines represent, respectively, the cases of γ=0°, 30° and 60°.

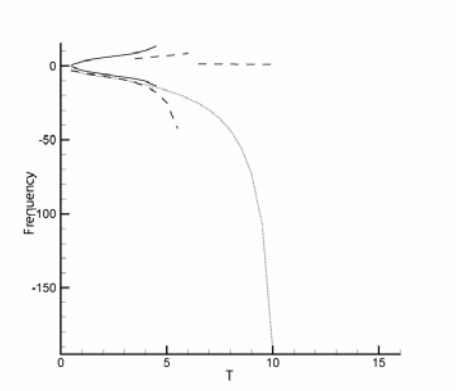

Figure 4. The same as in the figure 3 but for L=0.05.

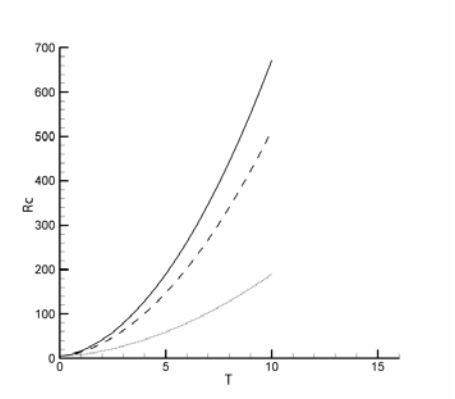

Figure 5. The same as in the figure 3 but for R_c instead of frequency.

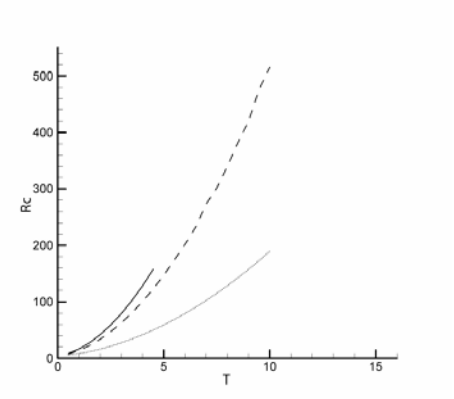

Figure 6. The same as in the figure 4 but for R_c instead of frequency.

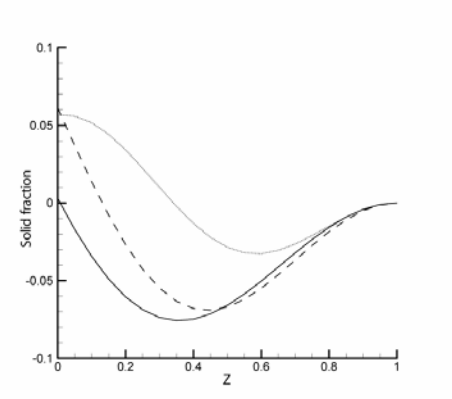

Figure 7. Perturbation to solid fraction versus z for L=0, K_1=1.0, G=2.0 and G_t=0.672. Here the solid, dashed and dotted lines present, respectively, the cases for (T, γ)= (0.0, 0°), (1.0, 0°) and (1.0, 60°).

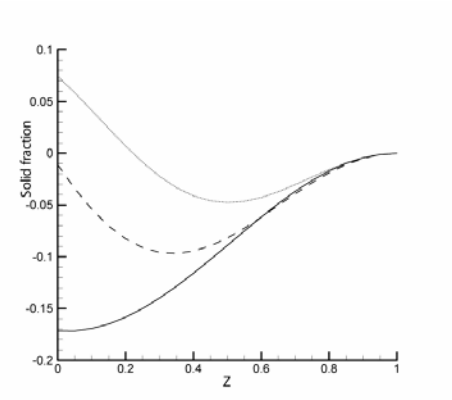

Figure 8. Perturbation to solid fraction versus z for L=0.05, G=2.0 and G_t =0.672. Here the solid, dashed and dotted lines present, respectively, the cases for (T, γ)= (0.0, 0°), (1.0, 0°) and (1.0, 60°).

List of Recent TAM Reports

No.	Authors	Title	Date
1004	Fried, E., and R. E. Todres	Normal-stress differences and the detection of disclinations in nematic elastomers—*Journal of Polymer Science B: Polymer Physics* **40**, 2098–2106 (2002)	June 2002
1005	Fried, E., and B. C. Roy	Gravity-induced segregation of cohesionless granular mixtures—*Lecture Notes in Mechanics*, in press (2002)	July 2002
1006	Tomkins, C. D., and R. J. Adrian	Spanwise structure and scale growth in turbulent boundary layers—*Journal of Fluid Mechanics* (submitted)	Aug. 2002
1007	Riahi, D. N.	On nonlinear convection in mushy layers: Part 2. Mixed oscillatory and stationary modes of convection—*Journal of Fluid Mechanics* **517**, 71–102 (2004)	Sept. 2002
1008	Aref, H., P. K. Newton, M. A. Stremler, T. Tokieda, and D. L. Vainchtein	Vortex crystals—*Advances in Applied Mathematics* **39**, in press (2002)	Oct. 2002
1009	Bagchi, P., and S. Balachandar	Effect of turbulence on the drag and lift of a particle—*Physics of Fluids*, in press (2003)	Oct. 2002
1010	Zhang, S., R. Panat, and K. J. Hsia	Influence of surface morphology on the adhesive strength of aluminum/epoxy interfaces—*Journal of Adhesion Science and Technology* **17**, 1685–1711 (2003)	Oct. 2002
1011	Carlson, D. E., E. Fried, and D. A. Tortorelli	On internal constraints in continuum mechanics—*Journal of Elasticity* **70**, 101–109 (2003)	Oct. 2002
1012	Boyland, P. L., M. A. Stremler, and H. Aref	Topological fluid mechanics of point vortex motions—*Physica D* **175**, 69–95 (2002)	Oct. 2002
1013	Bhattacharjee, P., and D. N. Riahi	Computational studies of the effect of rotation on convection during protein crystallization—*International Journal of Mathematical Sciences* **3**, 429–450 (2004)	Feb. 2003
1014	Brown, E. N., M. R. Kessler, N. R. Sottos, and S. R. White	*In situ* poly(urea-formaldehyde) microencapsulation of dicyclopentadiene—*Journal of Microencapsulation* (submitted)	Feb. 2003
1015	Brown, E. N., S. R. White, and N. R. Sottos	Microcapsule induced toughening in a self-healing polymer composite—*Journal of Materials Science* (submitted)	Feb. 2003
1016	Kuznetsov, I. R., and D. S. Stewart	Burning rate of energetic materials with thermal expansion—*Combustion and Flame* (submitted)	Mar. 2003
1017	Dolbow, J., E. Fried, and H. Ji	Chemically induced swelling of hydrogels—*Journal of the Mechanics and Physics of Solids*, in press (2003)	Mar. 2003
1018	Costello, G. A.	Mechanics of wire rope—Mordica Lecture, Interwire 2003, Wire Association International, Atlanta, Georgia, May 12, 2003	Mar. 2003
1019	Wang, J., N. R. Sottos, and R. L. Weaver	Thin film adhesion measurement by laser induced stress waves—*Journal of the Mechanics and Physics of Solids* (submitted)	Apr. 2003
1020	Bhattacharjee, P., and D. N. Riahi	Effect of rotation on surface tension driven flow during protein crystallization—*Microgravity Science and Technology* **14**, 36–44 (2003)	Apr. 2003
1021	Fried, E.	The configurational and standard force balances are not always statements of a single law—*Proceedings of the Royal Society* (submitted)	Apr. 2003
1022	Panat, R. P., and K. J. Hsia	Experimental investigation of the bond coat rumpling instability under isothermal and cyclic thermal histories in thermal barrier systems—*Proceedings of the Royal Society of London A* **460**, 1957–1979 (2003)	May 2003
1023	Fried, E., and M. E. Gurtin	A unified treatment of evolving interfaces accounting for small deformations and atomic transport: grain-boundaries, phase transitions, epitaxy—*Advances in Applied Mechanics* **40**, 1–177 (2004)	May 2003
1024	Dong, F., D. N. Riahi, and A. T. Hsui	On similarity waves in compacting media—*Horizons in World Physics* **244**, 45–82 (2004)	May 2003

List of Recent TAM Reports (cont'd)

No.	*Authors*	*Title*	*Date*
1025	Liu, M., and K. J. Hsia	Locking of electric field induced non-180° domain switching and phase transition in ferroelectric materials upon cyclic electric fatigue—*Applied Physics Letters* **83**, 3978–3980 (2003)	May 2003
1026	Liu, M., K. J. Hsia, and M. Sardela Jr.	In situ X-ray diffraction study of electric field induced domain switching and phase transition in PZT-5H—*Journal of the American Ceramics Society* (submitted)	May 2003
1027	Riahi, D. N.	On flow of binary alloys during crystal growth—*Recent Research Development in Crystal Growth* **3**, 49–59 (2003)	May 2003
1028	Riahi, D. N.	On fluid dynamics during crystallization—*Recent Research Development in Fluid Dynamics* **4**, 87–94 (2003)	July 2003
1029	Fried, E., V. Korchagin, and R. E. Todres	Biaxial disclinated states in nematic elastomers—*Journal of Chemical Physics* **119**, 13170–13179 (2003)	July 2003
1030	Sharp, K. V., and R. J. Adrian	Transition from laminar to turbulent flow in liquid filled microtubes—*Physics of Fluids* (submitted)	July 2003
1031	Yoon, H. S., D. F. Hill, S. Balachandar, R. J. Adrian, and M. Y. Ha	Reynolds number scaling of flow in a Rushton turbine stirred tank: Part I—Mean flow, circular jet and tip vortex scaling—*Chemical Engineering Science* (submitted)	Aug. 2003
1032	Raju, R., S. Balachandar, D. F. Hill, and R. J. Adrian	Reynolds number scaling of flow in a Rushton turbine stirred tank: Part II—Eigen-decomposition of fluctuation—*Chemical Engineering Science* (submitted)	Aug. 2003
1033	Hill, K. M., G. Gioia, and V. V. Tota	Structure and kinematics in dense free-surface granular flow—*Physical Review Letters* **91**, 064302 (2003)	Aug. 2003
1034	Fried, E., and S. Sellers	Free-energy density functions for nematic elastomers—*Journal of the Mechanics and Physics of Solids* **52**, 1671–1689 (2004)	Sept. 2003
1035	Kasimov, A. R., and D. S. Stewart	On the dynamics of self-sustained one-dimensional detonations: A numerical study in the shock-attached frame—*Physics of Fluids* (submitted)	Nov. 2003
1036	Fried, E., and B. C. Roy	Disclinations in a homogeneously deformed nematic elastomer—*Nature Materials* (submitted)	Nov. 2003
1037	Fried, E., and M. E. Gurtin	The unifying nature of the configurational force balance—*Mechanics of Material Forces* (P. Steinmann and G. A. Maugin, eds.), in press (2003)	Dec. 2003
1038	Panat, R., K. J. Hsia, and J. W. Oldham	Rumpling instability in thermal barrier systems under isothermal conditions in vacuum—*Philosophical Magazine*, in press (2004)	Dec. 2003
1039	Cermelli, P., E. Fried, and M. E. Gurtin	Sharp-interface nematic–isotropic phase transitions without flow—*Archive for Rational Mechanics and Analysis* **174**, 151–178 (2004)	Dec. 2003
1040	Yoo, S., and D. S. Stewart	A hybrid level-set method in two and three dimensions for modeling detonation and combustion problems in complex geometries—*Combustion Theory and Modeling* (submitted)	Feb. 2004
1041	Dienberg, C. E., S. E. Ott-Monsivais, J. L. Ranchero, A. A. Rzeszutko, and C. L. Winter	Proceedings of the Fifth Annual Research Conference in Mechanics (April 2003), TAM Department, UIUC (E. N. Brown, ed.)	Feb. 2004
1042	Kasimov, A. R., and D. S. Stewart	Asymptotic theory of ignition and failure of self-sustained detonations—*Journal of Fluid Mechanics* (submitted)	Feb. 2004
1043	Kasimov, A. R., and D. S. Stewart	Theory of direct initiation of gaseous detonations and comparison with experiment—*Proceedings of the Combustion Institute* (submitted)	Mar. 2004
1044	Panat, R., K. J. Hsia, and D. G. Cahill	Evolution of surface waviness in thin films via volume and surface diffusion—*Journal of Applied Physics* (submitted)	Mar. 2004
1045	Riahi, D. N.	Steady and oscillatory flow in a mushy layer—*Current Topics in Crystal Growth Research*, in press (2004)	Mar. 2004
1046	Riahi, D. N.	Modeling flows in protein crystal growth—*Current Topics in Crystal Growth Research*, in press (2004)	Mar. 2004

List of Recent TAM Reports (cont'd)

No.	*Authors*	*Title*	*Date*
1047	Bagchi, P., and S. Balachandar	Response of the wake of an isolated particle to isotropic turbulent cross-flow—*Journal of Fluid Mechanics* (submitted)	Mar. 2004
1048	Brown, E. N., S. R. White, and N. R. Sottos	Fatigue crack propagation in microcapsule toughened epoxy—*Journal of Materials Science* (submitted)	Apr. 2004
1049	Zeng, L., S. Balachandar, and P. Fischer	Wall-induced forces on a rigid sphere at finite Reynolds number—*Journal of Fluid Mechanics* (submitted)	May 2004
1050	Dolbow, J., E. Fried, and H. Ji	A numerical strategy for investigating the kinetic response of stimulus-responsive hydrogels—*Computer Methods in Applied Mechanics and Engineering* **194**, 4447–4480 (2005)	June 2004
1051	Riahi, D. N.	Effect of permeability on steady flow in a dendrite layer—*Journal of Porous Media*, in press (2004)	July 2004
1052	Cermelli, P., E. Fried, and M. E. Gurtin	Transport relations for surface integrals arising in the formulation of balance laws for evolving fluid interfaces—*Journal of Fluid Mechanics* (submitted)	Sept. 2004
1053	Stewart, D. S., and A. R. Kasimov	Theory of detonation with an embedded sonic locus—*SIAM Journal on Applied Mathematics* (submitted)	Oct. 2004
1054	Stewart, D. S., K. C. Tang, S. Yoo, M. Q. Brewster, and I. R. Kuznetsov	Multi-scale modeling of solid rocket motors: Time integration methods from computational aerodynamics applied to stable quasi-steady motor burning—*Proceedings of the 43rd AIAA Aerospace Sciences Meeting and Exhibit* (January 2005), Paper AIAA-2005-0357 (2005)	Oct. 2004
1055	Ji, H., H. Mourad, E. Fried, and J. Dolbow	Kinetics of thermally induced swelling of hydrogels—*International Journal of Solids and Structures* (submitted)	Dec. 2004
1056	Fulton, J. M., S. Hussain, J. H. Lai, M. E. Ly, S. A. McGough, G. M. Miller, R. Oats, L. A. Shipton, P. K. Shreeman, D. S. Widrevitz, and E. A. Zimmermann	Final reports: Mechanics of complex materials, Summer 2004 (K. M. Hill and J. W. Phillips, eds.)	Dec. 2004
1057	Hill, K. M., G. Gioia, and D. R. Amaravadi	Radial segregation patterns in rotating granular mixtures: Waviness selection—*Physical Review Letters* **93**, 224301 (2004)	Dec. 2004
1058	Riahi, D. N.	Nonlinear oscillatory convection in rotating mushy layers—*Journal of Fluid Mechanics*, in press (2005)	Dec. 2004
1059	Okhuysen, B. S., and D. N. Riahi	On buoyant convection in binary solidification—*Journal of Fluid Mechanics* (submitted)	Jan. 2005
1060	Brown, E. N., S. R. White, and N. R. Sottos	Retardation and repair of fatigue cracks in a microcapsule toughened epoxy composite—Part I: Manual infiltration—*Composites Science and Technology* (submitted)	Jan. 2005
1061	Brown, E. N., S. R. White, and N. R. Sottos	Retardation and repair of fatigue cracks in a microcapsule toughened epoxy composite—Part II: *In situ* self-healing—*Composites Science and Technology* (submitted)	Jan. 2005
1062	Berfield, T. A., R. J. Ong, D. A. Payne, and N. R. Sottos	Residual stress effects on piezoelectric response of sol-gel derived PZT thin films—*Journal of Applied Physics* (submitted)	Apr. 2005
1063	Anderson, D. M., P. Cermelli, E. Fried, M. E. Gurtin, and G. B. McFadden	General dynamical sharp-interface conditions for phase transformations in viscous heat-conducting fluids—*Journal of Fluid Mechanics* (submitted)	Apr. 2005
1064	Fried, E., and M. E. Gurtin	Second-gradient fluids: A theory for incompressible flows at small length scales—*Journal of Fluid Mechanics* (submitted)	Apr. 2005
1065	Gioia, G., and F. A. Bombardelli	Localized turbulent flows on scouring granular beds—*Physical Review Letters*, in press (2005)	May 2005

List of Recent TAM Reports (cont'd)

No.	*Authors*	*Title*	*Date*
1066	Fried, E., and S. Sellers	Orientational order and finite strain in nematic elastomers—*Journal of Chemical Physics* **123**, 044901 (2005)	May 2005
1067	Chen, Y.-C., and E. Fried	Uniaxial nematic elastomers: Constitutive framework and a simple application—*Proceedings of the Royal Society of London A*, in press (2005)	June 2005
1068	Fried, E., and S. Sellers	Incompatible strains associated with defects in nematic elastomers—*Journal of Chemical Physics*, in press (2005)	Aug. 2005
1069	Gioia, G., and X. Dai	Surface stress and reversing size effect in the initial yielding of ultrathin films—*Journal of Applied Mechanics*, in press (2005)	Aug. 2005
1070	Gioia, G., and P. Chakraborty	Turbulent friction in rough pipes and the energy spectrum of the phenomenological theory—*Physical Review Letters* **96**, 044502 (2006)	Aug. 2005
1071	Keller, M. W., and N. R. Sottos	Mechanical properties of capsules used in a self-healing polymer—*Experimental Mechanics* (submitted)	Sept. 2005
1072	Chakraborty, P., G. Gioia, and S. Kieffer	Volcán Reventador's unusual umbrella	Sept. 2005
1073	Fried, E., and S. Sellers	Soft elasticity is not necessary for striping in nematic elastomers—*Nature Physics* (submitted)	Sept. 2005
1074	Fried, E., M. E. Gurtin, and Amy Q. Shen	Theory for solvent, momentum, and energy transfer between a surfactant solution and a vapor atmosphere—*Physical Review E* (submitted)	Sept. 2005
1075	Chen, X., and E. Fried	Rayleigh–Taylor problem for a liquid–liquid phase interface—*Journal of Fluid Mechanics* (submitted)	Oct. 2005
1076	Riahi, D. N.	Mathematical modeling of wind forces—In *The Euler Volume* (Abington, UK: Taylor and Francis), in press (2005)	Oct. 2005
1077	Fried, E., and R. E. Todres	Mind the gap: The shape of the free surface of a rubber-like material in the proximity to a rigid contactor—*Journal of Elasticity*, in press (2006)	Oct. 2005
1078	Riahi, D. N.	Nonlinear compositional convection in mushy layers—*Journal of Fluid Mechanics* (submitted)	Dec. 2005
1079	Bhattacharjee, P., and D. N. Riahi	Mathematical modeling of flow control using magnetic fluid and field—In *The Euler Volume* (Abington, UK: Taylor and Francis), in press (2005)	Dec. 2005
1080	Bhattacharjee, P., and D. N. Riahi	A hybrid level set/VOF method for the simulation of thermal magnetic fluids—*International Journal for Numerical Methods in Engineering* (submitted)	Dec. 2005
1081	Bhattacharjee, P., and D. N. Riahi	Numerical study of surface tension driven convection in thermal magnetic fluids—*Journal of Crystal Growth* (submitted)	Dec. 2005
1082	Riahi, D. N.	Inertial and Coriolis effects on oscillatory flow in a horizontal dendrite layer—*Transport in Porous Media* (submitted)	Jan. 2006
1083	Wu, Y., and K. T. Christensen	Population trends of spanwise vortices in wall turbulence—*Journal of Fluid Mechanics* (submitted)	Jan. 2006
1084	Natrajan, V. K., and K. T. Christensen	The role of coherent structures in subgrid-scale energy transfer within the log layer of wall turbulence—*Physics of Fluids* (submitted)	Jan. 2006
1085	Wu, Y., and K. T. Christensen	Reynolds-stress enhancement associated with a short fetch of roughness in wall turbulence—*AIAA Journal* (submitted)	Jan. 2006
1086	Fried, E., and M. E. Gurtin	Cosserat fluids and the continuum mechanics of turbulence: A generalized Navier–Stokes-α equation with complete boundary conditions—*Journal of Fluid Mechanics* (submitted)	Feb. 2006
1087	Riahi, D. N.	Inertial effects on rotating flow in a porous layer—*Journal of Porous Media* (submitted)	Feb. 2006